

SEMDOT: Smooth-Edged Material Distribution for Optimizing Topology Algorithm

Yun-Fei Fu¹,
Bernard Rolfe¹,
Louis N. S. Chiu²,
Yanan Wang¹,
Xiaodong Huang³,
Kazem Ghabraie^{1*}

1. School of Engineering, Deakin University, Waurn Ponds, VIC 3217, Australia

2. Department of Materials Science and Engineering, Monash University, Clayton, VIC 3800,
Australia

3. Faculty of Science, Engineering and Technology, Swinburne University of Technology, Hawthorn,
VIC 3122, Australia

*E-mail: k.ghabraie@deakin.edu.au

Tel: +61 3 524 79574

Highlights

- Smooth-Edged Material Distribution for Optimizing Topology (SEMDOT) algorithm is presented.
- Effects of Heaviside smooth and step functions on SEMDOT are investigated.
- The benefits and distinctions of SEMDOT compared to well-established element-based algorithms are shown.

Abstract

Element-based topology optimization algorithms capable of generating smooth boundaries have drawn serious attention given the significance of accurate boundary information in engineering applications. The basic framework of a new element-based continuum algorithm has been proposed in this paper. This algorithm is based on a smooth-edged material distribution strategy that uses solid/void grid points assigned to each element. The named Smooth-Edged Material Distribution for Optimizing Topology (SEMDOT) algorithm uses elemental volume fractions which depend on the densities of grid points as design variables rather than elemental densities. SEMDOT is not only capable of obtaining optimized topologies with smooth and clear boundaries but also generally shows a better performance compared to other topology optimization methods. Several numerical examples are studied to demonstrate the application and effectiveness of SEMDOT. First, the advantages of using the Heaviside smooth function are discussed in comparison to the Heaviside step function. Then, the benefits of introducing two filters in this algorithm are shown. Finally, comparisons are conducted to exhibit the differences of SEMDOT with some well-established element-based algorithms.

Keywords: Topology optimization; Smooth design; Elemental volume fractions; Boundary elements; Heaviside smooth function

1 Introduction

Topology optimization basically aims to distribute a given amount of material within a predefined design domain such that optimal or near optimal structural performance can be obtained [1, 2, 3]. It often provides highly efficient designs that could not be obtained by simple intuition without assuming any prior structural configuration. Topology optimization as a design method has been greatly developed and extensively used since the pioneering paper on numerical topology optimization by Bendsøe and Kikuchi [4]. A number of topology optimization algorithms have been proposed based on different strategies: homogenization of microstructures [4], using elemental densities as design variables [5], evolutionary approaches [6, 7], topological derivative [8], level-set (LS) [9, 10, 11], phase field [12], moving morphable component (MMC) [13, 14, 15, 16], moving morphable void (MMV) [17, 18, 19], elemental volume fractions [20], and using the floating projection [21]. In recent years, these topology optimization approaches have been applied in a wide range of distinct engineering problems, including frequency responses [22, 23], stress problems [24, 25], convection problems [26, 27, 28], structural failure problems [29, 30, 31, 32], large-scale problems [33, 34, 35], nanophotonics [36], metamaterial design [37], and manufacturing oriented methods [38, 39, 40, 41, 42] have been presented in recent years.

Early proposed topology optimization algorithms are mainly element-based such as solid isotropic material with penalization (SIMP) algorithm [43, 44] and bi-directional evolutionary structural optimization (BESO) algorithm [45, 46, 47]. SIMP uses the artificial power-law function between elemental densities and material properties to suppress intermediate elements to a solution with black and white elements, and BESO heuristically updates design variables using discrete values (0 and 1). As elements are not only involved in finite element analysis (FEA) but the formation of topological boundaries, zigzag (for example, BESO) or both zigzag and blurry boundaries (for example, SIMP) will be inevitably generated. Therefore, shape optimization or other post-processing methods have to be used to obtain accurate boundary information after topology optimization [48, 49]. Given the significance of the accurate boundary representation, some proposed algorithms such as the level-set method, MMC-based method, elemental volume fractions based method, and using the floating projection have successfully solved the boundary issue. Even though there are a number of algorithms capable of forming smooth or high resolution boundaries, element-based algorithms that could combine the benefits of different methods are generally preferred because of their advantages of easy implementation and ability of searching a solution near the global optimum.

Elemental volume fractions based methods are originally from the evolutionary topology optimization (ETO) algorithms using the continuation method on the volume and BESO-based optimizer [20, 50, 51, 52]. To provide a more easy-to-use, flexible, and efficient optimization platform, the authors proposed a new smooth continuum topology optimization algorithm through combining the benefits of the smooth representation in ETO and density-based opti-

mization in SIMP [53, 54, 55, 56]. The proposed algorithm is termed Smooth-Edged Material Distribution for Optimizing Topology (SEMDOT) based on its optimization mechanism.

Compared with some newly developed or improved algorithms capable of generating smooth boundaries, SEMDOT can be easily integrated with some existing methods that were established based on SIMP to achieve specific performance goals. An example is the combination of SEMDOT and Langelaar’s additive manufacturing (AM) filter [57] which can successfully generate smooth self-supporting topologies [53, 55]. Other than Langelaar’s AM filter, some other strategies regarding AM restrictions proposed by van de Ven et al. [58] and Zhang et al. [59] can also be considered in SEMDOT for the support-free design. However, extra efforts have to be made for MMCs-based methods to obtain self-supporting designs [60]. In addition, the effectiveness of SEMDOT in solving 3D optimization problems is recently demonstrated by Fu et al. [56], through solving a number of benchmark problems and a comparison with a well-established large-scale topology optimization framework, TopOpt (proposed by Aage et al. [33]).

Even though the theoretical framework of SEMDOT was built and demonstrated by authors, other benefits and distinctions of SEMDOT compared with some current element-based algorithms have not been thoroughly discussed. Furthermore, details of SEMDOT algorithm and some of its subtle differences with methods like ETO which translate into more robust performance have not been discussed before.

In this work, the reason behind using the Heaviside smooth function in SEMDOT instead of the Heaviside step function that is extensively used in ETO algorithms is explained. Effects of different combinations of filter radii on performance, convergence, and topologies, which have not been discussed in authors’ previous works, are investigated, and numerical comparisons with other element-based topology optimization methods are conducted.

An overview of this paper is as follows. Section 2 explains the mathematical framework of SEMDOT. Section 3 conducts several numerical examples to exhibit the benefits and distinctions of SEMDOT compared with a number of element-based topology optimization algorithms. Concluding remarks are drawn in Section 4.

2 Formulation

2.1 Problem statements and sensitivity analysis

SEMDOT is based on the adoption of elemental volume fractions X_e as design variables of the optimization problem. Elemental volume fractions depend on the densities of grid points $\rho_{e,g}$ that is much finer than the adopted finite element discretization. The generation of smooth topological boundaries is based on the solid/void design of grid points that are assigned to each element, as illustrated in Figure 1. Even though the number of grid points is much higher than that of elements, grid points are not involved in finite element analysis (FEA). Hence,

SEMDOT can maintain a proper balance between the smoothness of topological boundaries and computational cost. The minimum compliance (the maximum stiffness) optimization problem, one of the most popular test cases for topology optimization, is considered in this paper, which can be stated as

$$\begin{aligned}
& \min : C(X_e) = \mathbf{f}^T \mathbf{u} \\
& \text{subject to : } \mathbf{K}(X_e) \mathbf{u} = \mathbf{f} \\
& \frac{\sum_{e=1}^M X_e V_e}{\sum_{e=1}^M V_e} - V^* \leq 0 \\
& 0 < \rho_{\min} \leq X_e \leq 1; \quad e = 1, 2, \dots, M
\end{aligned} \tag{1}$$

where C is the compliance of the topological design; \mathbf{f} and \mathbf{u} are global force and displacement vectors, respectively; \mathbf{K} is the global stiffness matrix; V_e is the volume of the e th element; V^* is the prescribed value of the allowable volume; M is the total number of elements in the design domain; ρ_{\min} is a small artificial parameter (for example, 0.001).

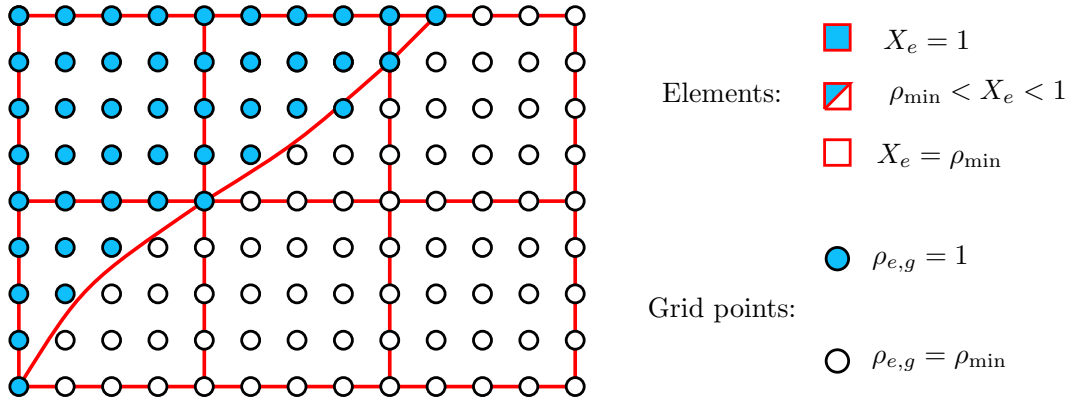


Figure 1: Illustration of smooth-edged material distribution

The elemental volume fraction is defined as

$$X_e = \frac{1}{N} \sum_{g=1}^N \rho_{e,g} \tag{2}$$

where N is the total number of grid points in each element. The following interpolation scheme is used for material properties of each element,

$$\begin{aligned}
E_e(X_e) &= (1 - X_e)E_e(\rho_{\min}) + X_e E_e(1) \\
&= (1 - X_e)\rho_{\min}^p E^1 + X_e E^1, \quad X_e \in [\rho_{\min}, 1]
\end{aligned} \tag{3}$$

where $E_e(X_e)$ is the interpolated Young's modulus of element e , expressed as a function of the elemental volume fraction of this element, X_e . E^1 is the Young's modulus of the solid material, and p is a penalty coefficient.

Based on the same representation in Equation 3, the elemental stiffness matrix can be expressed as

$$\begin{aligned}\mathbf{K}_e(X_e) &= (1 - X_e)\mathbf{K}_e^0 + X_e\mathbf{K}_e^1 \\ &= (1 - X_e)\rho_{\min}^p\mathbf{K}_e^1 + X_e\mathbf{K}_e^1, \quad X_e \in [\rho_{\min}, 1]\end{aligned}\quad (4)$$

where $\mathbf{K}_e(X_e)$ is the function of the stiffness matrix with respect to the elemental volume fraction X_e , \mathbf{K}_e^0 is the stiffness matrix of the void material, and \mathbf{K}_e^1 is the stiffness matrix of the solid material.

The sensitivity measures the effectiveness of altering elemental volume fractions on reducing or increasing the objective function through which the search direction of optimization can be determined [61, 62]. In SEMDOT, for the problem stated in Equation 1, sensitivities of elemental volume fractions can be approximated as

$$\begin{aligned}\frac{\partial C}{\partial X_e} &= (1 - X_e)\left.\frac{\partial C}{\partial X_e}\right|_{X_e=\rho_{\min}} + X_e\left.\frac{\partial C}{\partial X_e}\right|_{X_e=1} \\ &= -p[(1 - X_e)\rho_{\min}^{p-1} + X_e]\mathbf{u}_e^T\mathbf{K}_e^1\mathbf{u}_e, \quad X_e \in [\rho_{\min}, 1]\end{aligned}\quad (5)$$

where \mathbf{u}_e is the displacement vector of the e th element.

2.2 Filtering

Using filters in topology optimization is an effective way to ensure regularity or existence of topological designs [63, 64]. The basic idea of filters is to substitute a (possibly) non-regular function with its regularization [63, 64]. The filter that has the same form of the density filter is used for regularization of topology optimization problems in SEMDOT. The filtering technique for elemental volume fractions is expressed as [65, 66, 67]:

$$\tilde{X}_e = \frac{\sum_{l=1}^{N_e} \omega_{el} X_l}{\sum_{l=1}^{N_e} \omega_{el}} \quad (6)$$

where \tilde{X}_e is the filtered elemental volume fraction, N_e is the neighborhood set of elements within the filter domain for the e th element that is a circle centered at the centroid of this element with a predefined filter radius r_{\min} , and ω_{el} is a linear weight factor defined as

$$\omega_{el} = \max(0, r_{\min} - \Delta(e, l)) \quad (7)$$

where $\Delta(e, l)$ is the center-to-center distance of the l th element within the filter domain to the e th element. It is noted that the filter for elemental volume fractions (Equations 6 and 7) can be substituted by other filters that were developed based on standard SIMP such as the sensitivity filter presented by Sigmund [68] and the partial differential equation (PDE) filters proposed by Lazarov and Sigmund [63]. It should be noted that SEMDOT aims to obtain a topological

design with intermediate (gray) elements only along boundaries instead of pursuing a pure black and white (0/1) design, which means intermediate elements are useful for the determination of smooth boundaries. Consequently, some filters suppressing intermediate elements to black and white (0/1) elements (for example, Heaviside projection filter [69], morphology based filters [67], and volume preserving Heaviside projection scheme [70]) do not suit SEMDOT.

To obtain the densities of grid points, nodal densities should be obtained first in SEMDOT. Nodal densities can be obtained using a heuristic filter similar to the one presented in BESO [71, 72, 73, 74, 75]:

$$\rho_n = \frac{\sum_{e=1}^M \omega_{ne} \tilde{X}_e}{\sum_{e=1}^M \omega_{ne}} \quad (8)$$

where ρ_n is the density of the n th node and ω_{ne} is the weight factor defined as

$$\omega_{ne} = \max(0, \Upsilon_{\min} - \Delta(n, e)) \quad (9)$$

where $\Delta(n, e)$ is the distance between the n th node and the center of the e th element and Υ_{\min} is the heuristic filter radius. It is important that the heuristic filter radius Υ_{\min} in SEMDOT is set to a value not less than 1, otherwise topological designs cannot be obtained for most test cases.

In the ETO algorithm proposed by Chen et al. [50] and Li et al. [52], only Equation 8 was used for filtering, and good topological designs for phononic crystals were obtained. However, the successful implementation of this filtering strategy is due to the usage of a modified optimality criteria (OC) method and evolutionary framework. Generally, the sole use of the heuristic filter (Equation 8) is not sufficient in SEMDOT.

2.3 Generation of smooth topological boundaries

The density at the grid point $\rho(\zeta, \eta)$ in the e th element can be obtained through linear interpolation of nodal densities ρ_n . Considering a four-node element as an example, the density of the grid point $\rho(\zeta, \eta)$ is expressed by

$$\rho(\zeta, \eta) = \sum_{\gamma=1}^4 N^\gamma(\zeta, \eta) \rho_n^\gamma \quad \text{and} \quad \rho(\zeta, \eta) \in \rho(x, y) \quad (10)$$

where (ζ, η) is the local coordinate of the grid point, ρ_n^γ is the density for the γ th node of the element, and $N^\gamma(\zeta, \eta)$ is an appropriate shape function.

Theoretically, the solid/void design of grid points can be implemented by either Heaviside step function or Heaviside smooth function. The Heaviside step function is expressed by [69]

$$\rho_{e,g} = \begin{cases} 1 & \text{if } \rho_{e,g} > \Psi \\ \rho_{\min} & \text{if } \rho_{e,g} \leq \Psi \end{cases} \quad (11)$$

where Ψ is a threshold value.

The tanh-based expression of the Heaviside smooth function proposed by Wang et al. [76] is used in SEMDOT, which is

$$\rho_{e,g} = \frac{\tanh(\beta \cdot \Psi) + \tanh[\beta \cdot (\rho(x, y) - \Psi)]}{\tanh(\beta \cdot \Psi) + \tanh[\beta \cdot (1.0 - \Psi)]} \quad (12)$$

where β is a scaling parameter that controls the steepness and is updated by

$$\beta_k = \beta_{k-1} + \Lambda \quad (13)$$

where the subscripts denote the iteration number and Λ is the evolution rate for β .

Once grid point densities are calculated, design variables (filtered elemental volume fractions) are updated for the next round of FEA through summing up the grid points for each element:

$$\tilde{X}_e = \frac{1}{N} \sum_{g=1}^N \rho_{e,g}^{new} \quad (14)$$

where $\rho_{e,g}^{new}$ is the density of the grid point obtained by the Heaviside step or smooth function.

The shape of the topological design is represented by a level-set function $\Phi(x, y)$:

$$\Phi(x, y) = \begin{cases} \rho(x, y) - \Psi > 0 & \text{for solid region} \\ \rho(x, y) - \Psi = 0 & \text{for boundary} \\ \rho(x, y) - \Psi < 0 & \text{for void region} \end{cases} \quad (15)$$

where (x, y) is the global coordinate of grid points, $\Phi(x, y)$ is the level-set function for grid points, and $\rho(x, y)$ is the density of the grid point at (x, y) . Unlike the direct sensitivity-based level-set function presented by Da et al. [20] and Liu et al. [51], Equation 15 uses the densities of grid points that are determined originally based on sensitivity analysis (Equation 5). Therefore, Equation 15 can be regarded as an indirect sensitivity-based or grid point density based level-set function.

2.4 Convergence criteria

For BESO-based methods, the optimization procedure terminates when the average change of the objective function values in recent iterations is less than a prescribed tolerance value [77]. As previously mentioned by Sigmund and Maute [78], the convergence criterion of BESO could prematurely terminate the optimization procedure, because design variables may be in an oscillating state switching between 0 and 1 even though the objective function value based convergence criterion is satisfied. This oscillating state would result in a solution far from the optimum. On the other hand, the optimization procedure of standard SIMP is terminated when the maximum variation of design variables within two successive iterations is less than a prescribed tolerance [79]. However, when solving an optimization problem with a large number of elements, convergence difficulties can be observed in SIMP, as is discussed in Section 3.3.

If the Heaviside step function is considered in SEMDOT, the optimization procedure terminates when the overall topological alteration is less than its predefined tolerance value, which can be stated as:

$$\frac{\sum_{e=1}^M |X_e^k - X_e^{k-1}|}{\sum_{e=1}^M X_e^k} \leq \tau \quad (16)$$

where τ is the tolerance value for the overall topological alteration. This convergence criterion (Equation 16) is based on the overall measure of the variation of design variables compared to the local measure used in SIMP, and its better performance in determining convergence had been demonstrated by Fu et al. [53, 55, 56]. It is noted that Equation 16 can also be used in SIMP or BESO and is likely to improve their determination of termination point.

When the Heaviside smooth function is considered, one additional termination criterion should be introduced as the Heaviside smooth function will inevitably cause the topological boundary error during the optimization process. The topological boundary error convergence criterion that measures the accuracy of the level-set function representing the smooth topological boundary is defined as:

$$\frac{N_v}{M} \leq \epsilon; \quad (17)$$

where N_v is the number of intermediate elements that are not along boundaries, M is the total number of elements, and ϵ is the tolerance value for the topological boundary error.

In comparison to the Heaviside smooth function (Equation 12), the Heaviside step function (Equation 11) will not cause the topological boundary error, but it can cause numerical instabilities in SEMDOT, as is discussed in Section 3.1.

2.5 Optimization procedure

The optimization procedure of SEMDOT mainly consists of two parts: the implementation of structural changes based on elemental volume fractions and the generation of smooth topological boundaries based on the solid/void design of grid points. The improved and simplified flowchart of SEMDOT, which is based on the flowchart presented by Fu et al. [55], is illustrated in Figure 2.

3 Numerical Experiments

Benchmark 2D optimization problems are solved to demonstrate the validity of SEMDOT and exhibit the differences between SEMDOT and some existing algorithms: SIMP, BESO, and ETO. The prescribed value of the allowable volume V^* is set to 0.3. For all numerical examples, an isotropic linear elastic material model is assumed with Young's modulus of $E = 1$ MPa and Poisson's ratio of $\mu = 0.3$. Following Fu et al. [56], $\beta_0 = 0.5$ and $\Lambda = 0.5$ are employed in the Heaviside smooth function (Equation 12), and the penalty coefficient of $p = 1.5$ is used

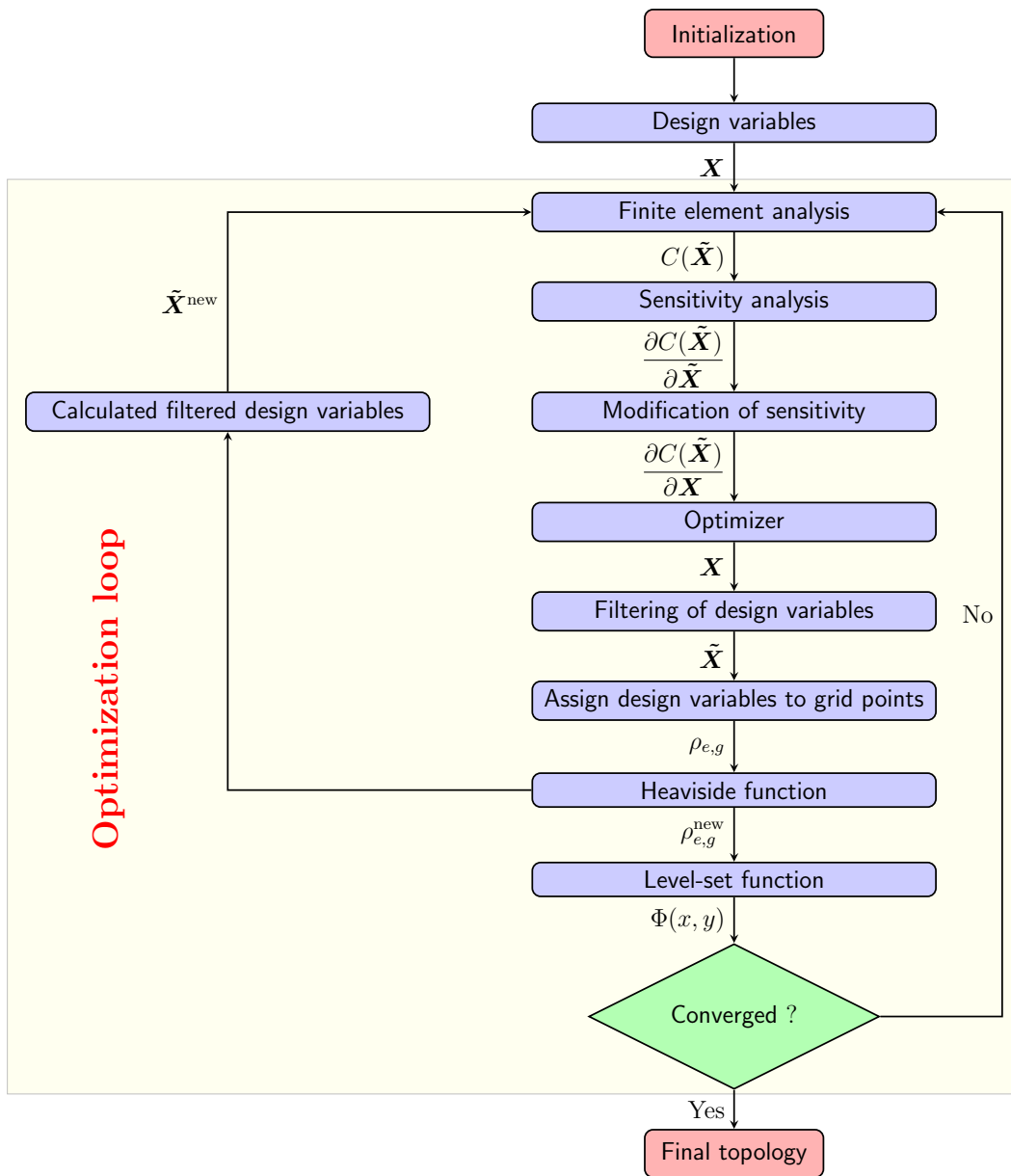


Figure 2: Flowchart of the SEMDOT method

in SEMDOT. The tolerance values of $\epsilon = 0.001$ and $\tau = 0.001$ are used in the convergence criteria. A grid with $10 \times 10 \times 10$ points in each element is used. Unless otherwise stated, the heuristic filter radius Υ_{\min} is set to 1. In addition, the method of moving asymptotes (MMA) proposed by Svanberg [80] is used to update design variables, and default parameters in MMA are adopted.

3.1 Effects of Heaviside functions

A simply supported deep beam subjected to a unit vertical load ($F = -1\text{N}$) at its bottom center is considered to investigate the influences of the Heaviside step and smooth functions on the topological design, performance, and convergency of SEMDOT. The design domain and boundary condition are shown in Figure 3. The bottom left corner is hinged, and the vertical displacement at the bottom right corner is prevented. A 180×90 mesh is used, and the filter radius r_{\min} is set to 2 time elements width.

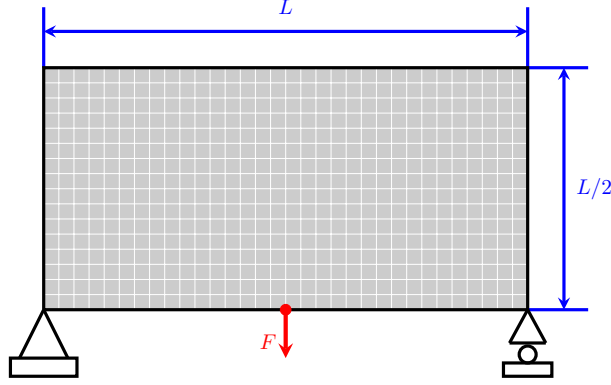


Figure 3: Design domain of a simply supported deep beam

The convergence history in Figure 4a shows that great fluctuations appear in the initial 20 iterations when the Heaviside step function is used. These fluctuations are associated with scattered material resulting in complicated topologies (Figures 4b and 4c), meaning that the Heaviside step function has the difficulty in extracting topological boundaries at the early stages of optimization. Afterwards, the optimization process steadily converges at 21.3875 J after 167 iterations and later topologies are reasonable (Figures 4d to 4g). Compared to the Heaviside step function, the Heaviside smooth function does not cause any numerical instabilities, and therefore the whole optimization process steadily converges at 21.1049 J after 142 iterations (Figure 5a). As shown in Figure 5a, the topological boundary error gradually decreases to almost 0% when the converged topology is obtained. Two different final topologies obtained by Heaviside step and smooth functions are shown in Figures 4g and 5b, respectively. In this case, the Heaviside smooth function performs better than the Heaviside step function both in compliance and convergence.

In some engineering problems, certain areas of the design domain are required to be void (non-design areas) during the whole optimization process. Another version of this problem

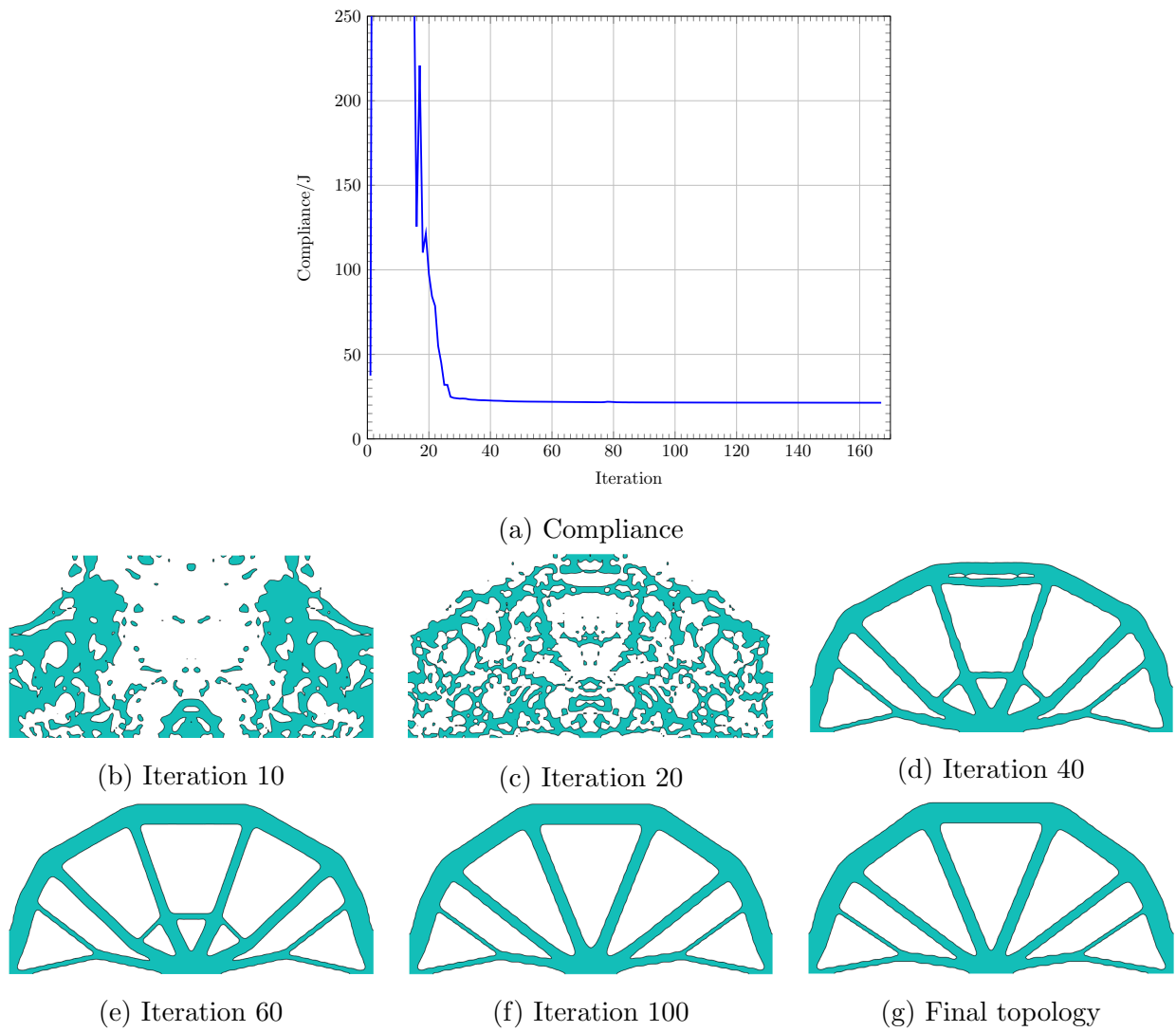


Figure 4: Compliance and optimized topology obtained with Heaviside step function for simply supported deep beam case

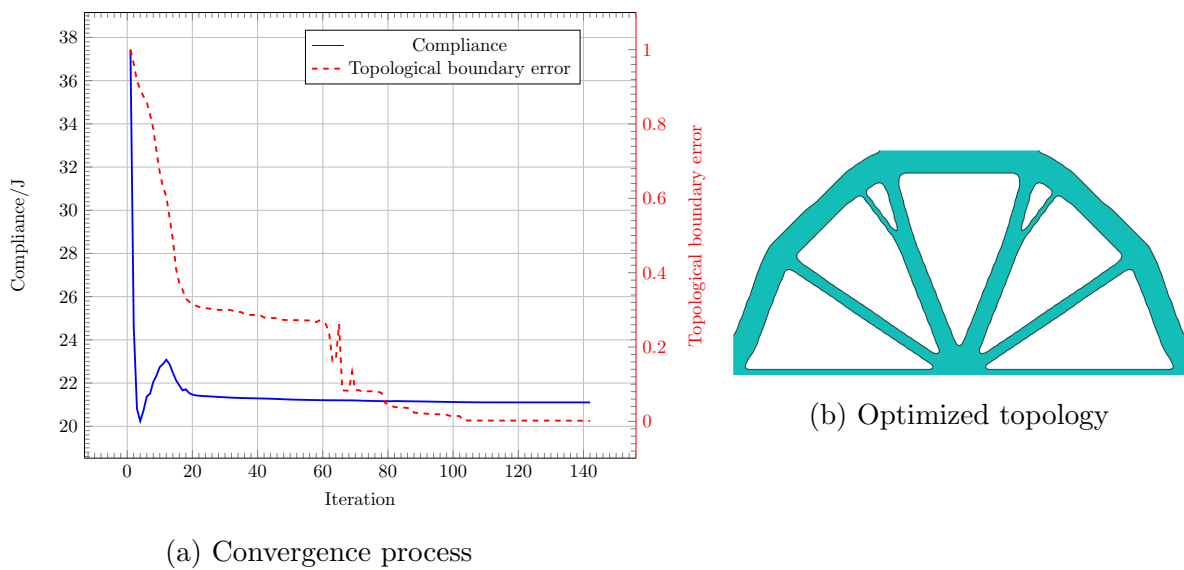


Figure 5: Convergence process and optimized topology obtained with Heaviside smooth function for simply supported deep beam case

with a non-designable circular hole with a radius of $L/6$ and a center located at $(L/2, L/4)$ as illustrated in Figure 6 is used to further test the performance of Heaviside step and smooth functions in SEMDOT. All parameter settings remain unchanged.

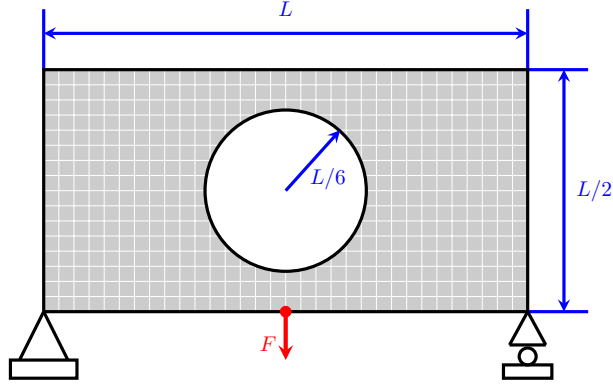


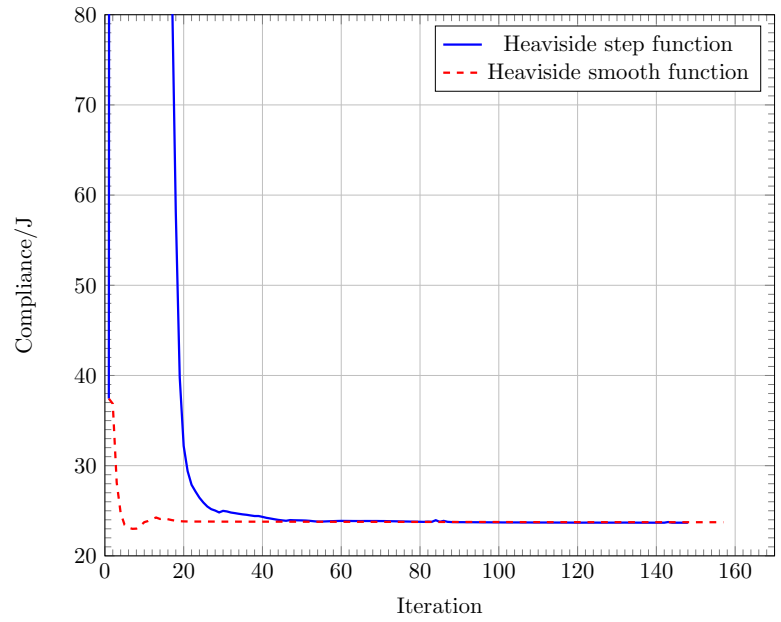
Figure 6: Design domain of a simply supported deep beam with a fixed hole

Figure 7a shows that SEMDOT using the Heaviside step function converges after 148 iterations, which is a little less than when the Heaviside smooth function is used (157). However, like the previous case, great fluctuations appear at the early stages of optimization when the Heaviside step function is used. Converged compliance is 23.6741 J for the Heaviside step function and 23.7306 J for the Heaviside smooth function, so the difference is negligible (around 0.2%). In this case, the Heaviside step function performs a little better than the Heaviside smooth function in compliance and convergence. However, the asymmetric topology obtained by the Heaviside step function has several tiny holes and one thin bar shown by a red circle in Figure 7b. This design cannot be easily manufactured even with AM [53]. By contrast, the symmetric topology obtained by the Heaviside smooth function has better manufacturability (Figure 7c).

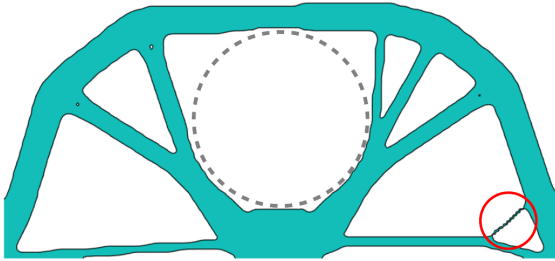
Based on the above discussions, it is concluded that the Heaviside smooth function is more suitable than the Heaviside step function for SEMDOT despite requiring an additional termination criterion (Equation 17). Therefore, the Heaviside smooth function will be used for the rest of numerical experiments in this paper rather than the Heaviside step function.

3.2 Effects of filter radii

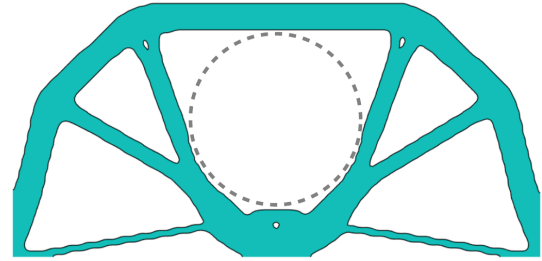
Two combinations of filter radii (i.e., $r_{\min} = 3$, $\Upsilon_{\min} = 3$ and $r_{\min} = 3$, $\Upsilon_{\min} = 1$) were used in authors' previous works [53, 54, 55, 56]. Other than those two combinations, different combinations of filter radii can also be considered in optimizing topologies with SEMDOT, which provides more design freedom for designers. The so-called MesserschmidtBlkowBlohm (MBB) beam is used here to demonstrate the effects of the two filter radii, r_{\min} and Υ_{\min} , on performance, convergency, and topological designs. The design domain and boundary conditions are shown in Figure 8. Only half of the MBB beam is considered as the design domain due to symmetry. As illustrated in Figure 8, the symmetric boundary condition is applied to the left



(a) Convergence histories



(b) Optimized topology obtained with Heaviside step function



(c) Optimized topology obtained with Heaviside smooth function

Figure 7: Comparisons of performance, convergency, and topological designs between Heaviside step and smooth functions for simply supported deep beam case with a fixed hole

side; the vertical displacement at the bottom right corner is restricted; and a unit vertical load ($F=-1$ N) is applied at the top left corner. The design domain is discretized by a 150×50 finite element mesh.

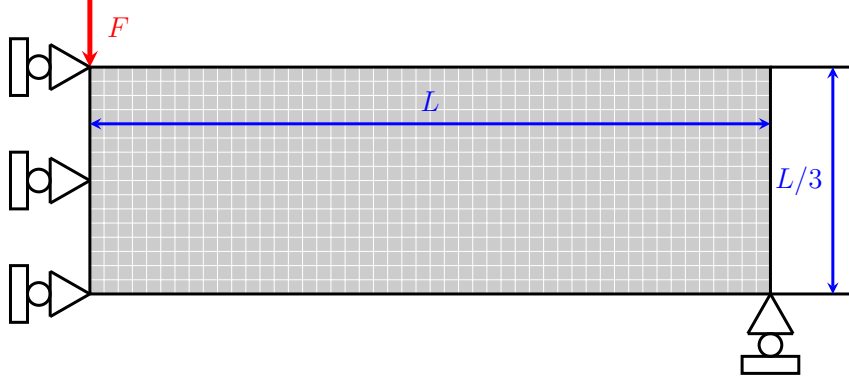


Figure 8: Design domain of half an MBB beam

Figure 9a shows that the highest compliance (287.2474 J) is obtained when the combination of $r_{\min} = 1$ and $\Upsilon_{\min} = 2.8$ is used. This drops to 283.7538 J when the combination of $r_{\min} = 2.8$ and $\Upsilon_{\min} = 1$ is used, meaning that Υ_{\min} will cause worse results than r_{\min} . Generally, increasing either r_{\min} or Υ_{\min} can contribute to the rise of compliance, and then a relatively stable value can be reached when either r_{\min} or Υ_{\min} is large enough. Figure 9b shows that using high values of Υ_{\min} will prolong the convergence process more than using high values of r_{\min} , and the highest number of iterations (378) is obtained when $r_{\min} = 2.6$ and $\Upsilon_{\min} = 3$.

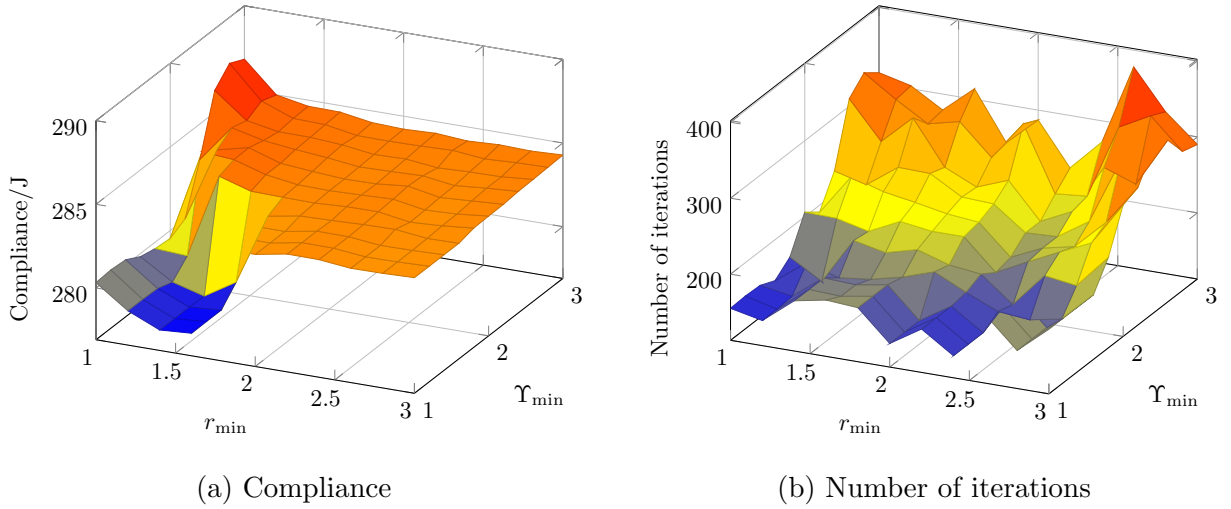


Figure 9: Compliance and number of iterations for different values of r_{\min} and Υ_{\min} solving MBB beam case

Figure 10 shows that increasing either r_{\min} or Υ_{\min} results in simpler topologies with less holes. Small holes vanish when the combination of $r_{\min} = 3$ and $\Upsilon_{\min} = 3$ is used, which is beneficial to the manufacturability of optimized topologies. Figure 11 shows the compliance, convergence, and topological designs under large values of r_{\min} and $\Upsilon_{\min}=1$. As topological

designs from $r_{\min} = 3.5$ have the similar structural layout with no small holes, only the topology at $r_{\min} = 3.5$ and $\Upsilon_{\min}=1$ is given in Figure 11 for simplicity. Compliance and the number of iterations of the combination of $r_{\min} = 3.5$ and $\Upsilon_{\min} = 1$ are 284.3535 J and 274, respectively, which are close to those of the combination of $r_{\min} = 3$ and $\Upsilon_{\min} = 3$ (284.2814 J and 290, respectively). There is an overall tendency for compliance to increase with r_{\min} (Figure 11). When r_{\min} reaches 3.9 and 4, large numbers of iterations (627 and 606, respectively) are required to reach convergence, as shown in Figure 11.

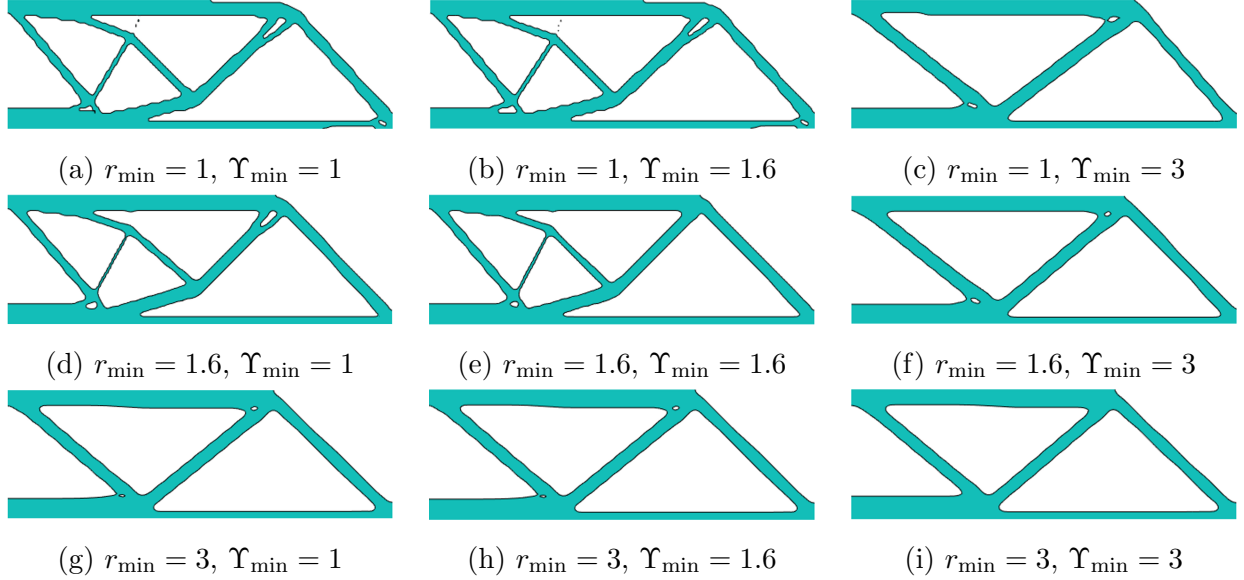


Figure 10: Optimized topologies with different combinations of r_{\min} and Υ_{\min} for MBB beam case

Even though Equation 6 is basically used for filtering elemental volume fractions in SEM-DOT, and the main function of Equation 8 is to assign elemental volume fractions to grid points, different combinations of r_{\min} and Υ_{\min} can also be considered in SEMDOT to explore different topological designs with better performance, quick convergence, or both. Generally, the fixed value of $\Upsilon_{\min}=1$ is recommended for the convenience of implementation.

3.3 Numerical comparisons

Two test cases (cantilever beam and L-bracket beam) are used to thoroughly compare SEM-DOT with some well-established element-based algorithms in the ability of seeking the optimal solution and convergency. In this comparison, only methods with published source codes (i.e., SIMP [81], BESO [73], and ETO [20]) are selected. In terms of SIMP, two typical filters: the density filter [65, 66, 67] and the Heaviside projection filter [69] are considered. In the Heaviside projection filter, the parameter controlling the smoothness of the approximation is gradually increased from 1 to 128 by doubling its value every 25 iterations or when the change between two consecutive designs is less than 0.01. For simplicity, SIMP-D and SIMP-H are used to represent SIMP with density and Heaviside projection filters, respectively, in graph legends

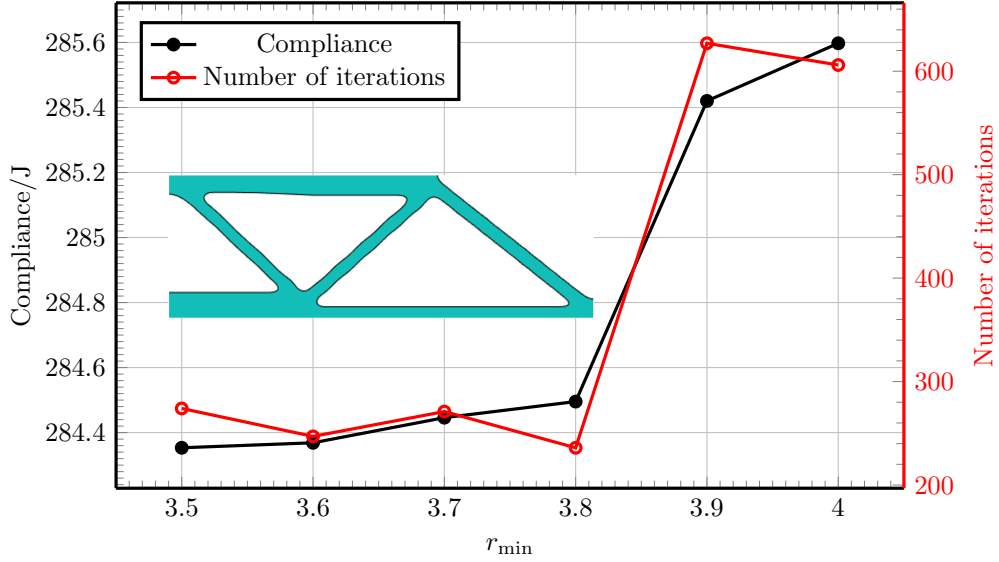


Figure 11: Compliance, convergence, and topological designs under large values of r_{\min} and $\Upsilon_{\min}=1$

and captions. The penalty coefficient of 1.5 is used in SEMDOT and ETO, and the penalty coefficient of 3 is used in SIMP and BESO. For BESO and ETO, the evolution rate er is set to 2%. In addition, the maximum number of iterations is set to 300 for all methods.

The design domain and boundary condition of a deep cantilever beam are shown in Figure 12. The left side is fixed and a unit vertical load ($F = -1\text{N}$) is imposed at the center point of the right side. The design domain of this beam is discretized by a 150×100 finite element mesh. The filter radius r_{\min} is set to 2.5 time elements width.

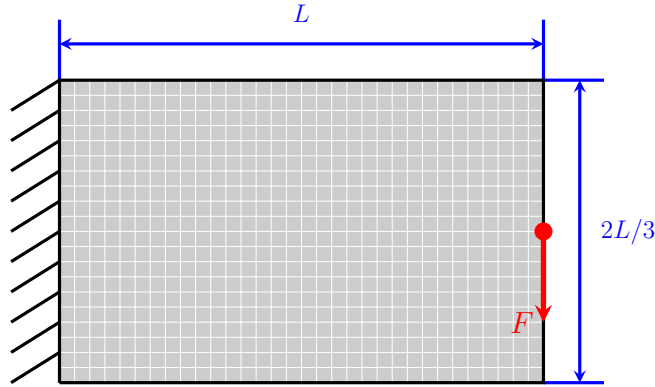


Figure 12: Design domain of a deep cantilever beam

Figure 13a shows that the best compliance (49.6856 J) is obtained by ETO, followed by 51.1240 J obtained by SEMDOT. The optimization process of ETO converges after 95 iterations, which is less than that of SEMDOT (123 iterations). Even though both SEMDOT and ETO are based on elemental volume fractions, optimized topologies (Figures 13b and 13f) are different. The topological design obtained by SEMDOT is similar to those obtained by SIMP (Figures 13c and 13d), and the topological design obtained by ETO is similar to that of BESO (Figure

13e). In this case, ETO is superior to SEMDOT in performance and convergence.

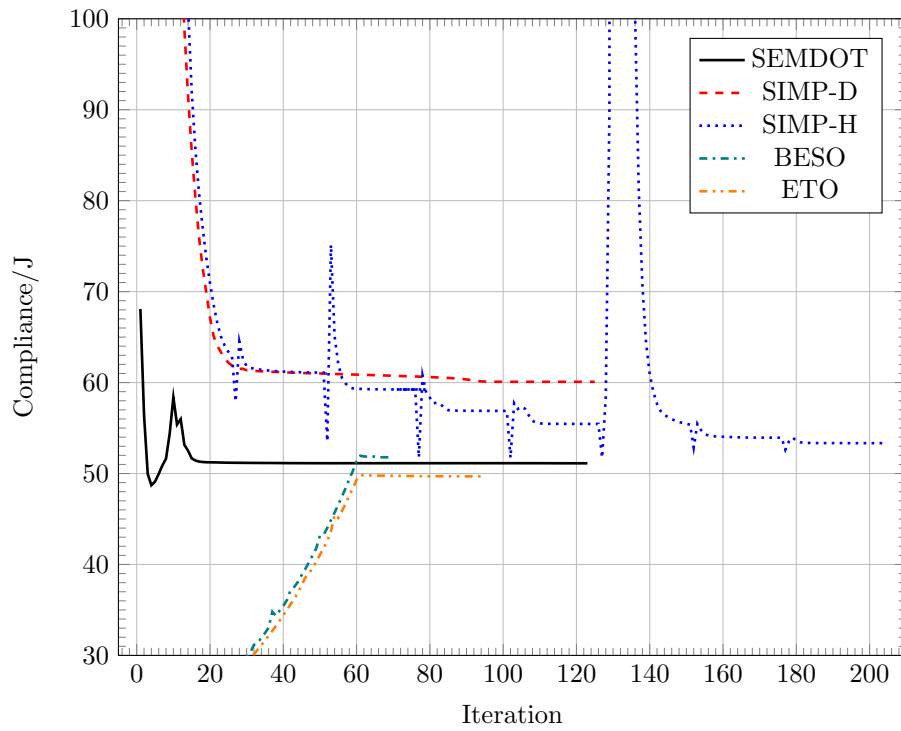
The worst compliance (60.0841 J) is obtained by SIMP with the density filter. This is because intermediate elements are allowed to distribute across the whole design domain, and intermediate elements result in smaller improvement of stiffness per density due to the use of penalty factor. Technically, it is difficult for the Heaviside projection filter to completely eliminate intermediate elements, however, there is almost no intermediate density element in the final result obtained by this method. BESO results in a pure black and white solution. BESO converges at the compliance of 51.7538 J after 69 iterations, which is better than SIMP with the Heaviside projection filter with $C=53.3355$ J after 204 iterations.

The second test case is an L-bracket, for which the design domain and boundary condition are shown in Figure 14. Here L is set to 400 element width. The top edge is fixed, and a unit vertical load ($F = -1\text{N}$) is applied at the top corner of the right side. The filter radius r_{\min} is set to 4 time elements width.

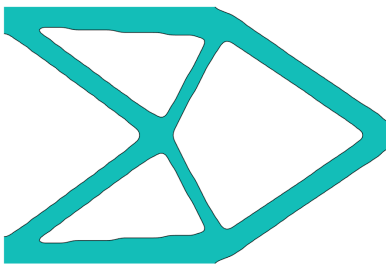
In this example, the best compliance (228.9422 J) is obtained by SEMDOT, followed by 249.2654 J obtained by ETO (Figure 15a). The optimization process of ETO converges after 79 iterations, which is still less than that of SEMDOT (181 iterations). Both SIMP algorithms face difficulties in convergence when the fine mesh is used, so optimization processes terminate after reaching the preset maximum number of iterations (300). By contrast, optimization processes of SEMDOT, BESO, and ETO converge within 200 iterations. Interestingly, as is evident from Figure 15a, numerical instabilities occur in the initial 10 iterations of the optimization process of SEMDOT despite using the Heaviside smooth function. This is because of the use of a large non-designable passive area that interferes with the determination of the topological boundary at the early stages of optimization. If the design domain can be defined explicitly, those numerical instabilities can be avoided. Afterwards, the optimization process quickly settles to a steady pass.

Unlike SEMDOT and SIMP (Figures 15b to 15d), BESO and ETO are prone to resulting in topological designs with thin features (Figures 15e and 15f), which are not preferred from the manufacturing point of view despite using the same value for the filter radius.

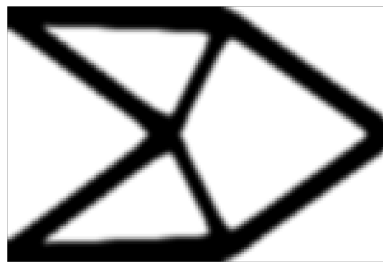
Although BESO shows the fastest convergency in these two test cases, this may be because of the premature termination mentioned in Section 2.4, and the same issue seems to occur in ETO because of using the same termination criterion. Otherwise, BESO and ETO could have the potential to obtain better performance. ETO converges slower than BESO as it uses elemental volume fractions as design variables instead of elemental densities. On the contrary, SEMDOT converges faster than SIMP because of distributing intermediate elements only along boundaries and introducing new termination criteria (Equations 16 and 17).



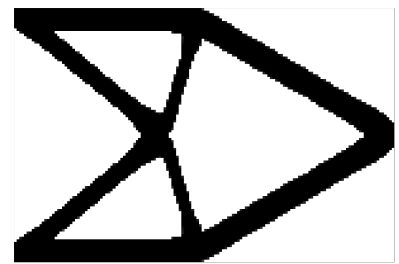
(a) Convergence histories



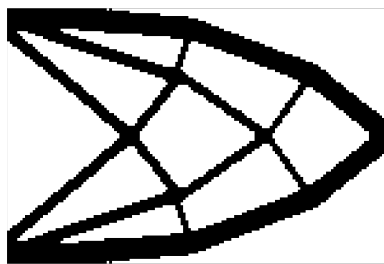
(b) SEMDOT



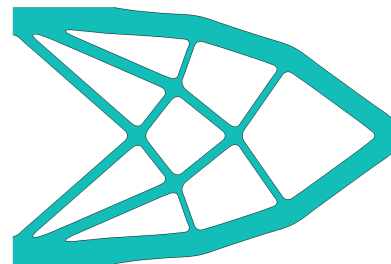
(c) SIMP-D



(d) SIMP-H



(e) BESO



(f) ETO

Figure 13: Comparisons of performance, convergency, and topological designs between different algorithms for deep cantilever beam case

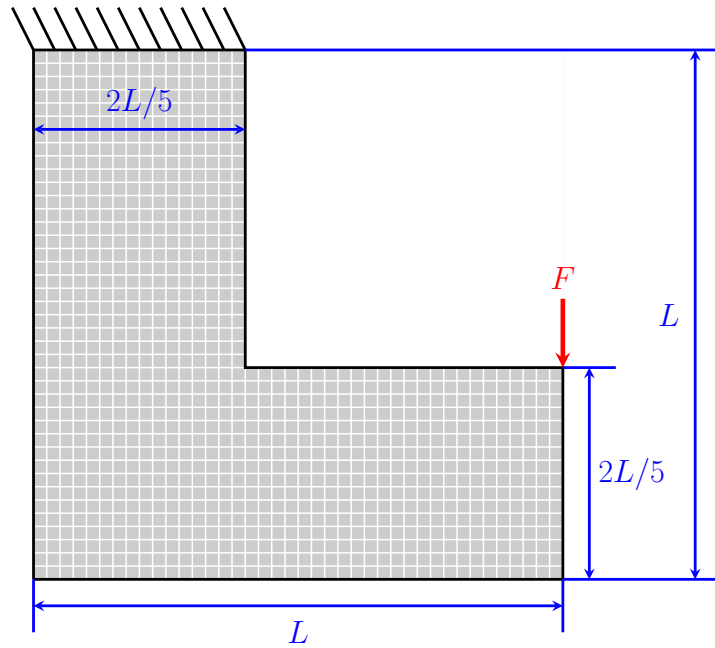


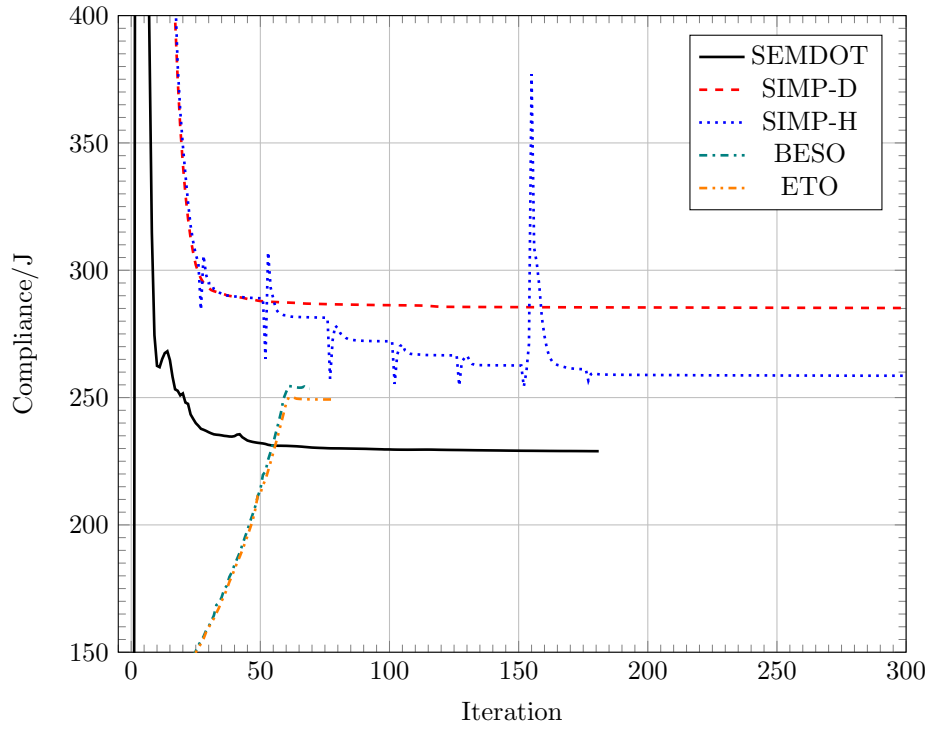
Figure 14: Design domain of an L-bracket beam

4 Conclusions

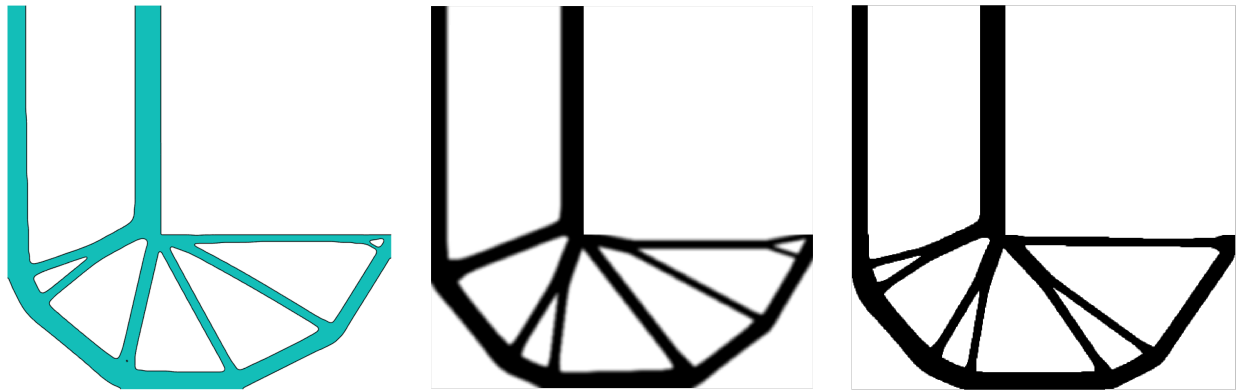
This paper explains the algorithm mechanism of SEMDOT using several numerical examples. Performance of SEMDOT is demonstrated through numerical comparisons with a range of well-established element-based algorithms. Concluding remarks can be stated as follows:

- The Heaviside smooth function is more suitable than the Heaviside step function for SEMDOT to obtain a more robust algorithm.
- The use of two filters enhances the flexibility of SEMDOT in exploring better performance and different topological designs.
- Even though SEMDOT is developed based on the SIMP framework, its convergency is stronger than standard SIMP because of its improved termination criteria.
- SEMDOT is capable of obtaining topological designs comparable or better than standard element-based algorithms such as SIMP and BESO or the newly developed ETO.

Even though this paper shows some benefits of SEMDOT, it should be acknowledged that when the same number of elements is used, the computational cost of SEMDOT would be higher than that of SIMP because of having to deal with extra grid points. It also should be acknowledged that SEMDOT is not a pioneering algorithm like SIMP, BESO, level-set method, MMC-based method, and using the floating projection. Instead, SEMDOT is an easy-to-use, flexible, and efficient optimization platform, which can be easily integrated with some existing approaches and solutions, particularly the ones developed for SIMP.



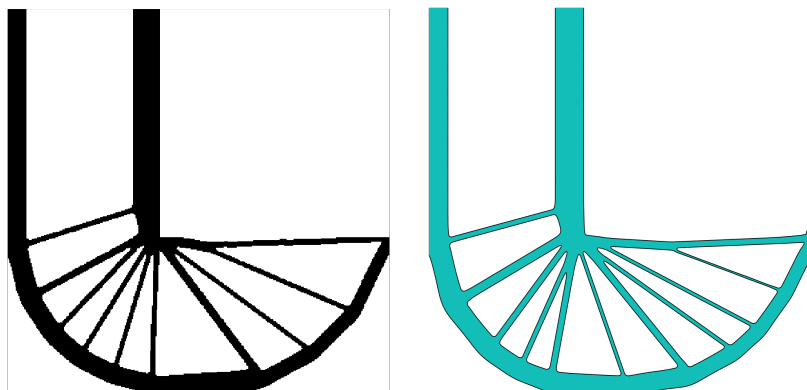
(a) Convergence histories



(b) SEMDOT

(c) SIMP-D

(d) SIMP-H



(e) BESO

(f) ETO

Figure 15: Comparisons of performance, convergency, and topological designs between different algorithms for L-bracket beam

As the level-set function (Equation 15) is used to extract the topological boundary, the open source framework for integrated AM and level-set-based topology optimization proposed by Vogiatzis et al. [82, 83] can be directly used to transfer the geometrical information of optimized topologies obtained by SEMDOT to STereoLithography (STL) files for further numerical analysis or AM. This capacity merged with its flexibility in adopting existing approaches makes SEMDOT a good tool for engineers who want to use the power of topology optimization to enhance their designs.

Funding

This research received no external funding.

Acknowledgements

The authors would like to thank Prof. Krister Svanberg for providing the MMA optimizer code. Mr. Yun-Fei Fu would like to thank Dr. Joe Alexandersen, University of Southern Denmark, for his suggestions on the mathematical statement of SEMDOT and Dr. Hongxin Wang, Hunan University, for his assistance on BESO test cases.

Conflicts of Interest

The authors declare that they have no known competing financial interests or personal relationships that could have appeared to influence the work reported in this paper.

References

- [1] Z. H. Zuo, Y. M. Xie, A simple and compact Python code for complex 3D topology optimization, *Advances in Engineering Software* 85 (2015) 1–11.
- [2] L. N. S. Chiu, B. Rolfe, X. H. Wu, W. Y. Yan, Effect of stiffness anisotropy on topology optimisation of additively manufactured structures, *Engineering Structures* 171 (2018) 842–848.
- [3] N. Pollini, O. Sigmund, C. S. Andreasen, J. Alexandersen, A poor mans approach for high-resolution three-dimensional topology design for natural convection problems, *Advances in Engineering Software* 140 (2020) 102736.
- [4] M. P. Bendsøe, N. Kikuchi, Generating optimal topologies in structural design using a homogenization method, *Computer Methods in Applied Mechanics and Engineering* 71 (1988) 197–224.

- [5] M. P. Bendsøe, Optimal shape design as a material distribution problem, *Structural and Multidisciplinary Optimization* 1 (1989) 193–202.
- [6] Y. M. Xie, G. P. Steven, Shape and layout optimization via an evolutionary procedure, in: *Proceedings of International Conference on Computational Engineering Science*, Hong Kong, 1992, p. 471.
- [7] Y. M. Xie, G. P. Steven, A simple evolutionary procedure for structural optimization, *Computers & Structures* 49 (1993) 885–896.
- [8] J. Sokolowski, A. Zochowski, On the topological derivative in shape optimization, *SIAM Journal on Control and Optimization* 37 (1999) 1251–1272.
- [9] G. Allaire, F. Jouve, A. M. Toader, A level-set method for shape optimization, *Comptes Rendus Mathematique* 334 (2002) 1125–1130.
- [10] G. Allaire, F. Jouve, A. M. Toader, Structural optimization using sensitivity analysis and a level-set method, *Journal of Computational Physics* 194 (2004) 363–393.
- [11] M. Y. Wang, X. M. Wang, D. M. Guo, A level set method for structural topology optimization, *Computer Methods in Applied Mechanics and Engineering* 192 (2003) 227–246.
- [12] B. Bourdin, A. Chambolle, Design-dependent loads in topology optimization, *ESAIM: Control, Optimisation and Calculus of Variations* 9 (2003) 19–48.
- [13] X. Guo, W. S. Zhang, W. L. Zhong, Doing topology optimization explicitly and geometrically—A new moving morphable components based framework, *Journal of Applied Mechanics* 81 (2014) 081009.
- [14] X. Guo, W. S. Zhang, J. Zhang, J. Yuan, Explicit structural topology optimization based on moving morphable components (MMC) with curved skeletons, *Computer Methods in Applied Mechanics and Engineering* 310 (2016) 711–748.
- [15] W. S. Zhang, J. Yuan, J. Zhang, X. Guo, A new topology optimization approach based on Moving Morphable Components (MMC) and the ersatz material model, *Structural and Multidisciplinary Optimization* 53 (2016) 1243–1260.
- [16] W. S. Zhang, D. Li, J. Yuan, J. F. Song, X. Guo, A new three-dimensional topology optimization method based on moving morphable components (MMCs), *Computational Mechanics* 59 (2017) 647–665.
- [17] W. S. Zhang, W. Y. Yang, J. H. Zhou, D. Li, X. Guo, Structural topology optimization through explicit boundary evolution, *Journal of Applied Mechanics* 84 (2017).

- [18] W. S. Zhang, J. S. Chen, X. F. Zhu, J. H. Zhou, D. C. Xue, X. Lei, X. Guo, Explicit three dimensional topology optimization via Moving Morphable Void (MMV) approach, *Computer Methods in Applied Mechanics and Engineering* 322 (2017) 590–614.
- [19] W. S. Zhang, D. D. Li, P. Kang, X. Guo, S. K. Youn, Explicit topology optimization using IGA-based moving morphable void (MMV) approach, *Computer Methods in Applied Mechanics and Engineering* 360 (2020) 112685.
- [20] D. C. Da, L. Xia, G. Y. Li, X. D. Huang, Evolutionary topology optimization of continuum structures with smooth boundary representation, *Structural and Multidisciplinary Optimization* 57 (2018) 2143–2159.
- [21] X. D. Huang, Smooth topological design of structures using the floating projection, *Engineering Structures* 208 (2020) 110330.
- [22] Z. D. Ma, N. Kikuchi, I. Hagiwara, Structural topology and shape optimization for a frequency response problem, *Computational Mechanics* 13 (1993) 157–174.
- [23] Z. H. Zuo, Y. M. Xie, X. D. Huang, Evolutionary topology optimization of structures with multiple displacement and frequency constraints, *Advances in Structural Engineering* 15 (2012) 359–372.
- [24] C. Le, J. Norato, T. Bruns, C. Ha, D. Tortorelli, Stress-based topology optimization for continua, *Structural and Multidisciplinary Optimization* 41 (2010) 605–620.
- [25] D. M. De Leon, J. Alexandersen, J. S. Fonseca, O. Sigmund, Stress-constrained topology optimization for compliant mechanism design, *Structural and Multidisciplinary Optimization* 52 (2015) 929–943.
- [26] J. Alexandersen, N. Aage, C. S. Andreasen, O. Sigmund, Topology optimisation for natural convection problems, *International Journal for Numerical Methods in Fluids* 76 (2014) 699–721.
- [27] J. Alexandersen, O. Sigmund, N. Aage, Large scale three-dimensional topology optimisation of heat sinks cooled by natural convection, *International Journal of Heat and Mass Transfer* 100 (2016) 876–891.
- [28] J. Asmussen, J. Alexandersen, O. Sigmund, C. S. Andreasen, A poor mans approach to topology optimization of natural convection problems, *Structural and Multidisciplinary Optimization* 59 (2019) 1105–1124.
- [29] E. Holmberg, B. Torstenfelt, A. Klarbring, Fatigue constrained topology optimization, *Structural and Multidisciplinary Optimization* 50 (2014) 207–219.

- [30] S. H. Jeong, D. H. Choi, G. H. Yoon, Fatigue and static failure considerations using a topology optimization method, *Applied Mathematical Modelling* 39 (2015) 1137–1162.
- [31] K. Nabaki, J. H. Shen, X. D. Huang, Evolutionary topology optimization of continuum structures considering fatigue failure, *Materials & Design* 166 (2019) 107586.
- [32] H. X. Wang, J. Liu, G. L. Wen, Y. M. Xie, The robust fail-safe topological designs based on the von Mises stress, *Finite Elements in Analysis and Design* 171 (2020) 103376.
- [33] N. Aage, E. Andreassen, B. S. Lazarov, Topology optimization using PETSc: An easy-to-use, fully parallel, open source topology optimization framework, *Structural and Multidisciplinary Optimization* 51 (2015) 565–572.
- [34] N. Aage, B. S. Lazarov, Parallel framework for topology optimization using the method of moving asymptotes, *Structural and Multidisciplinary Optimization* 47 (2013) 493–505.
- [35] H. X. Wang, J. Liu, G. L. Wen, An efficient evolutionary structural optimization method for multi-resolution designs, *Structural and Multidisciplinary Optimization* (2020) 1–17. doi:<https://doi.org/10.1007/s00158-020-02536-0>.
- [36] J. S. Jensen, O. Sigmund, Topology optimization for nano-photonics, *Laser & Photonics Reviews* 5 (2011) 308–321.
- [37] W. Chen, X. D. Huang, Topological design of 3D chiral metamaterials based on couple-stress homogenization, *Journal of the Mechanics and Physics of Solids* 131 (2019) 372–386.
- [38] J. K. Liu, Y. S. Ma, A survey of manufacturing oriented topology optimization methods, *Advances in Engineering Software* 100 (2016) 161–175.
- [39] S. L. Vatanabe, T. N. Lippi, C. R. de Lima, G. H. Paulino, E. C. Silva, Topology optimization with manufacturing constraints: A unified projection-based approach, *Advances in Engineering Software* 100 (2016) 97–112.
- [40] M. Langelaar, Topology optimization for multi-axis machining, *Computer Methods in Applied Mechanics and Engineering* 351 (2019) 226–252.
- [41] B. Barroqueiro, A. Andrade-Campos, R. Valente, Designing self supported SLM structures via topology optimization, *Journal of Manufacturing and Materials Processing* 3 (2019) 68.
- [42] H. C. Yu, H. J. Hong, S. Cao, R. Ahmad, Topology optimization for multipatch fused deposition modeling 3D printing, *Applied Sciences* 10 (2020) 943.
- [43] O. Sigmund, J. Petersson, Numerical instabilities in topology optimization: A survey on procedures dealing with checkerboards, mesh-dependencies and local minima, *Structural Optimization* 16 (1998) 68–75.

- [44] M. P. Bendsøe, O. Sigmund, *Topology Optimization Theory, Method and Applications*, 2nd ed., Springer-Verlag, Berlin Heidelberg, 2004.
- [45] X. Y. Yang, Y. M. Xie, G. P. Steven, O. M. Querin, Bidirectional evolutionary method for stiffness optimization, *AIAA Journal* 37 (1999) 1483–1488.
- [46] O. M. Querin, G. P. Steven, Y. M. Xie, Evolutionary structural optimisation (ESO) using a bidirectional algorithm, *Engineering Computations* 15 (1998) 1031–1048.
- [47] O. M. Querin, V. Young, G. P. Steven, Y. M. Xie, Computational efficiency and validation of bi-directional evolutionary structural optimisation, *Computer Methods in Applied Mechanics and Engineering* 189 (2000) 559–573.
- [48] K. Ghabraie, Y. M. Xie, X. D. Huang, G. Ren, Shape and reinforcement optimization of underground tunnels, *Journal of Computational Science and Technology* 4 (2010) 51–63.
- [49] K. Ghabraie, R. Chan, X. D. Huang, Y. M. Xie, Shape optimization of metallic yielding devices for passive mitigation of seismic energy, *Engineering Structures* 32 (2010) 2258–2267.
- [50] Y. F. Chen, F. Meng, G. Y. Li, X. D. Huang, Topology optimization of photonic crystals with exotic properties resulting from dirac-like cones, *Acta Materialia* 164 (2019) 377–389.
- [51] B. S. Liu, D. Guo, C. Jiang, G. Y. Li, X. D. Huang, Stress optimization of smooth continuum structures based on the distortion strain energy density, *Computer Methods in Applied Mechanics and Engineering* 343 (2019) 276–296.
- [52] W. B. Li, F. Meng, Y. F. Li, X. D. Huang, Topological design of 3D phononic crystals for ultra-wide omnidirectional bandgaps, *Structural and Multidisciplinary Optimization* 60 (2019) 2405–2415.
- [53] Y. F. Fu, B. Rolfe, N. S. L. Chiu, Y. N. Wang, X. D. Huang, K. Ghabraie, Design and experimental validation of self-supporting topologies for additive manufacturing, *Virtual and Physical Prototyping* 14 (2019) 382–394.
- [54] Y. F. Fu, B. Rolfe, N. S. L. Chiu, Y. N. Wang, X. D. Huang, K. Ghabraie, Topology optimization of continuum structures using smooth boundary representation, in: *13th World Congress on Structural and Multidisciplinary Optimization*, Beijing, China, 2019.
- [55] Y. F. Fu, B. Rolfe, N. S. L. Chiu, Y. N. Wang, X. D. Huang, K. Ghabraie, Parametric studies and manufacturability experiments on smooth self-supporting topologies, *Virtual and Physical Prototyping* 15 (2020) 22–34.

- [56] Y. F. Fu, B. Rolfe, N. S. L. Chiu, Y. N. Wang, X. D. Huang, K. Ghabraie, Smooth Topological Design of 3D Continuum Structures using Elemental Volume Fractions, *Computers and Structures* 231 (2020) 106213.
- [57] M. Langelaar, An additive manufacturing filter for topology optimization of print-ready designs, *Structural and Multidisciplinary Optimization* 55 (2017) 871–883.
- [58] E. van de Ven, R. Maas, C. Ayas, M. Langelaar, F. van Keulen, Continuous front propagation-based overhang control for topology optimization with additive manufacturing, *Structural and Multidisciplinary Optimization* 57 (2018) 2075–2091.
- [59] K. Q. Zhang, G. D. Cheng, L. Xu, Topology optimization considering overhang constraint in additive manufacturing, *Computers & Structures* 212 (2019) 86–100.
- [60] X. Guo, J. H. Zhou, W. S. Zhang, Z. L. Du, C. Liu, Y. Liu, Self-supporting structure design in additive manufacturing through explicit topology optimization, *Computer Methods in Applied Mechanics and Engineering* 323 (2017) 27–63.
- [61] K. Ghabraie, An improved soft-kill BESO algorithm for optimal distribution of single or multiple material phases, *Structural and Multidisciplinary Optimization* 52 (2015) 773–790.
- [62] K. Ghabraie, The ESO method revisited, *Structural and Multidisciplinary Optimization* 51 (2015) 1211–1222.
- [63] B. S. Lazarov, O. Sigmund, Filters in topology optimization based on Helmholtz-type differential equations, *International Journal for Numerical Methods in Engineering* 86 (2011) 765–781.
- [64] K. Svanberg, H. Svård, Density filters for topology optimization based on the pythagorean means, *Structural and Multidisciplinary Optimization* 48 (2013) 859–875.
- [65] B. Bourdin, Filters in topology optimization, *International Journal for Numerical Methods in Engineering* 50 (2001) 2143–2158.
- [66] T. E. Bruns, D. A. Tortorelli, Topology optimization of non-linear elastic structures and compliant mechanisms, *Computer Methods in Applied Mechanics and Engineering* 190 (2001) 3443–3459.
- [67] O. Sigmund, Morphology-based black and white filters for topology optimization, *Structural and Multidisciplinary Optimization* 33 (2007) 401–424.
- [68] O. Sigmund, On the design of compliant mechanisms using topology optimization, *Journal of Structural Mechanics* 25 (1997) 493–524.

- [69] J. K. Guest, J. H. Prévost, T. Belytschko, Achieving minimum length scale in topology optimization using nodal design variables and projection functions, *International Journal for Numerical Methods in Engineering* 61 (2004) 238–254.
- [70] S. L. Xu, Y. W. Cai, G. D. Cheng, Volume preserving nonlinear density filter based on heaviside functions, *Structural and Multidisciplinary Optimization* 41 (2010) 495–505.
- [71] X. D. Huang, Y. M. Xie, Convergent and mesh-independent solutions for the bi-directional evolutionary structural optimization method, *Finite Elements in Analysis and Design* 43 (2007) 1039–1049.
- [72] X. D. Huang, Y. M. Xie, Bi-directional evolutionary topology optimization of continuum structures with one or multiple materials, *Computational Mechanics* 43 (2009) 393–401.
- [73] X. D. Huang, Y. M. Xie, A further review of ESO type methods for topology optimization, *Structural and Multidisciplinary Optimization* 41 (2010) 671–683.
- [74] X. D. Huang, Y. M. Xie, Evolutionary topology optimization of continuum structures with an additional displacement constraint, *Structural and Multidisciplinary Optimization* 40 (2010) 409.
- [75] X. D. Huang, Y. M. Xie, Evolutionary topology optimization of continuum structures including design-dependent self-weight loads, *Finite Elements in Analysis and Design* 47 (2011) 942–948.
- [76] F. W. Wang, B. S. Lazarov, O. Sigmund, On projection methods, convergence and robust formulations in topology optimization, *Structural and Multidisciplinary Optimization* 43 (2011) 767–784.
- [77] L. Xia, Q. Xia, X. D. Huang, Y. M. Xie, Bi-directional evolutionary structural optimization on advanced structures and materials: A comprehensive review, *Archives of Computational Methods in Engineering* 25 (2018) 437–478.
- [78] O. Sigmund, K. Maute, Topology optimization approaches: A comparative review, *Structural and Multidisciplinary Optimization* 48 (2013) 1031–1055.
- [79] O. Sigmund, A 99 line topology optimization code written in Matlab, *Structural and Multidisciplinary Optimization* 21 (2001) 120–127.
- [80] K. Svanberg, The method of moving asymptotes (MMA) with some extensions, in: G. I. N. Rozvany (Ed.), *Optimization of Large Structural Systems*, Springer, Dordrecht: Kluwer, 1993, pp. 555–566.

- [81] E. Andreassen, A. Clausen, M. Schevenels, B. S. Lazarov, O. Sigmund, Efficient topology optimization in MATLAB using 88 lines of code, *Structural and Multidisciplinary Optimization* 43 (2011) 1–16.
- [82] P. Vogiatzis, S. K. Chen, C. Zhou, A MATLAB code for integrated additive manufacturing and level-set based topology optimization, in: *ASME 2016 International Design Engineering Technical Conferences and Computers and Information in Engineering Conference*, American Society of Mechanical Engineers, Charlotte, North Carolina, 2016, p. V02BT03A016.
- [83] P. Vogiatzis, S. K. Chen, C. Zhou, An open source framework for integrated additive manufacturing and level-set-based topology optimization, *Journal of Computing and Information Science in Engineering* 17 (2017) 041012.